

Constraints on N_{eff} of high energy non-thermal neutrino injections upto $z \sim 10^8$ from CMB spectral distortions and abundance of light elements

Sandeep Kumar Acharya,^a Rishi Khatri^a

^a*Department of Theoretical Physics, Tata Institute of Fundamental Research, Mumbai 400005, India*

E-mail: sandeepkumar@theory.tifr.res.in, khatri@theory.tifr.res.in

ABSTRACT: High energy neutrinos and anti-neutrinos ($\gtrsim 100$ GeV) can inject energetic electromagnetic particles into the baryon-photon plasma in the high redshift universe through electroweak showers from electroweak bremsstrahlung, inelastic scattering with the background electrons and nucleons, and by pair-production of standard model particles on background neutrinos and anti-neutrinos. In this paper, we evolve the particle cascades of high energy non-thermal neutrinos injections, using dark matter decay as a specific example, including relevant collision processes of these neutrinos with the background particles and taking into account the expansion of the universe. We study the effect of these non-thermal neutrino injections on the CMB spectral shape and abundance of light elements produced in the big bang nucleosynthesis. We show that CMB spectral distortions and abundance of light elements can constrain neutrino energy density at the recombination, parameterized as contribution to N_{eff} , from high energy neutrino injection. These constraints are stronger by several orders of magnitudes compared to the CMB anisotropy constraints. We also show that CMB spectral distortions can probe neutrino injections to significantly higher redshifts ($z > 2 \times 10^6$) as compared to pure electromagnetic energy injection.

1 Introduction

Precise measurement of the cosmic microwave background anisotropy (CMB) [1] has not only established the standard cosmological model with 6 parameters but it has also allowed us to study extensions of the standard model with extra parameters. One such extension is the energy density in free streaming relativistic particles usually parameterized by effective number of neutrino species (N_{eff}) defined using the CMB energy density as reference. The current $2\text{-}\sigma$ constraint on N_{eff} from CMB anisotropy is 2.92 ± 0.36 [1]. The standard model prediction for N_{eff} is 3.046 [2–12], for a more recent calculation see [13]. The extra relativistic energy density affects the expansion rate of the Universe. This makes N_{eff} somewhat degenerate with the Hubble parameter. By requiring the angular measure of the acoustic scale at the recombination epoch to be fixed (which is precisely measured by *Planck* [1]), constraints on the Hubble parameter lead to constraints on the total radiation energy density of the universe at the recombination epoch i.e. on the N_{eff} parameter. The extra neutrino species which are thermalized, in addition to the standard model neutrinos, or other new relativistic particles such as dark radiation can make $N_{\text{eff}} > 3.046$ while addition of extra energy to photons after neutrino decoupling can decrease the relative energy density in neutrinos with respect to the CMB and hence make $N_{\text{eff}} < 3.046$. However, we need not restrict ourselves to such scenarios involving new particles. We will consider the case where the extra N_{eff} is contributed by the energetic standard model neutrinos. One example is high energy non-thermal neutrino injections from dark matter decay in the pre-recombination era.

In almost all previous studies, it is assumed that the standard model interactions of neutrinos with the background particles are too weak to be important for any cosmological signature with the exception of their effect on BBN [7]. While this may be true of low energy neutrinos, energetic neutrinos above the W, Z boson mass scale can emit electromagnetic particles through electroweak showers from electroweak bremsstrahlung [14–16], inelastic scattering of injected neutrinos with the background nucleons (proton and helium nuclei) and electrons [17–19], and pair production of standard model particles by annihilation of injected neutrinos/anti-neutrinos with background anti-neutrinos and neutrinos [20, 21]. If the injected neutrino’s (anti-neutrino’s) energy is sufficiently high then it can pair produce electron-positron pairs and quark pairs on background anti-neutrinos (neutrinos). The quarks after hadronization and pion decay produce secondary electromagnetic particles and neutrinos. These electromagnetic particles, in the pre-recombination era, can produce CMB spectral distortion or modify the abundance of primordial elements.

Electromagnetic energy injection into the background baryon-photon plasma modifies the Planckian CMB spectrum, creating a distortion in the spectral shape. Assuming this distortion to be created by interaction of non-relativistic thermal electrons, heated by energy injection to the baryon-photon fluid, energy injection at $z \lesssim 2 \times 10^6$ leads to y , i , and μ -type (yim collectively) spectral distortions [22–28]. Recently, it was shown that at $z \lesssim 2 \times 10^5$, spectral distortion shapes (non-thermal relativistic or ntr -type) from high energy photon/electron injection can be substantially different from yim -type distortions [29, 30]. High energy pho-

ton/electron injection gives rise to a particle cascade. Particles in the time-evolving cascade can have relativistic energy which give rise to richer spectral distortion shapes as compared to *yim*-distortions. For energy injection at $z \gtrsim 2 \times 10^5$, *ntr*-spectral distortions also thermalize to μ -distortion [30]. While photon production processes such as bremsstrahlung and double Compton scattering are inefficient at $z \lesssim 2 \times 10^6$, their increasing efficiency above this redshift, in the thermalization epoch or blackbody photosphere, wash out any spectral distortion from electromagnetic energy injection and create a Planck spectrum with modified temperature. The transition from μ distortion to a temperature shift is captured by the μ -visibility function [23, 25, 31, 32]. The weakness of neutrino interactions implies that they deposit their energy gradually. In particular, neutrinos injected at $z \gtrsim 2 \times 10^6$ will deposit some of their energy in the photon-baryon plasma at $z \lesssim 2 \times 10^6$ and leave imprints in CMB spectral distortions. We thus have a new window into the thermalization epoch where any signature of direct electromagnetic energy injection is wiped out from the CMB. In general, for any energy injection process at $z \gtrsim 2 \times 10^6$, the electromagnetic part of the injected energy will be thermalized and will be invisible, except as contribution to the CMB energy density or a change in N_{eff} , while a fraction of energy injected in neutrinos will be deposited later and will be visible as CMB spectral distortions.

Injection of energetic photons above the photo-dissociation threshold of deuterium and helium can change the abundance of primordial elements. Given the precise measurements of abundance of elements, subject to astrophysical uncertainties, we can constrain electromagnetic energy injection upto redshifts $z \sim 3 \times 10^6$ [33–40]. The energetic photons can dissociate nuclei or can scatter with background electrons through Compton scattering, scatter with the CMB photons elastically, or pair produce electrons and positrons. Pair-production on the CMB photons is the dominant process when it is kinematically allowed. Since the energy of CMB photons increases with redshift ($\propto (1+z)$), the threshold energy of injected photons to pair-produce e^-e^+ decreases with redshift. When the pair-production threshold on the CMB photons is below helium photo-dissociation threshold of 19.81 MeV, most of the injected photons immediately pair-produce e^-e^+ and the pair-produced particles are not energetic enough to dissociate helium nuclei. This happens at $z \sim 3 \times 10^6$ and the constraints from photo-dissociation of BBN elements become weaker at $z \gtrsim 3 \times 10^6$. We can probe higher redshifts with deuterium destruction (photo-dissociation threshold=2.2 MeV), but constraints from deuterium destruction are much weaker due to its low abundance [35].

A sufficiently energetic neutrino above the quark pair production threshold releases ≈ 50 percent of its energy in electromagnetic particles [41] and the rest as secondary neutrinos. Assuming these secondary neutrinos do not pair produce, they will lose some of their energy to the baryon-photon plasma through various scattering processes and their remaining energy can be parameterized by N_{eff} . The electromagnetic energy deposition at $2 \times 10^5 \lesssim z \lesssim 2 \times 10^6$ gives rise to μ -distortions and the energy in μ distortion is constrained to be smaller than $\approx 10^{-4}$ of the CMB energy density ($\mu \lesssim 9 \times 10^5$) [42–44]. This means that N_{eff} from high energy neutrino injections is also constrained to be of the order of 10^{-4} of the CMB energy density, which is many orders magnitude stronger than the current CMB anisotropy constraints. The

CMB anisotropy constraints are of course more general while the CMB spectral distortion constraints are very model dependent and apply only to neutrinos with energy $\gtrsim 100$ GeV. Similar analysis can also be done for modification to the abundance of primordial elements.

For neutrinos with energy below the pair-production threshold of quarks with background anti-neutrinos but above the W, Z boson mass also, CMB spectral distortions and abundance of light elements can give reasonably stronger constraints compared to *Planck*, as we will show. For CMB spectral distortion constraints many orders of magnitude improvements is possible with future experiments such as Primordial Inflation Explorer (PIXIE) [45, 46].

Modification to the abundance of primordial elements from high energy neutrino injection was previously considered in [47, 48] (see also [49]). However, their analysis was limited to neutrino energy of 1 GeV- 10^3 GeV. Also, electroweak shower from neutrinos due to electroweak bremsstrahlung and inelastic scattering with background nucleons and electrons were not considered. In this paper, we consider neutrino injection from 10 GeV to 10^{12} GeV from dark matter decay. Detection of PeV neutrinos at *IceCube* [50] has inspired many particle physics models [51–54] in which dark matter can decay to high energy neutrinos. We consider monochromatic neutrino injection and evolve the neutrino spectrum from the redshift of energy injection upto the recombination epoch, taking into account the aforementioned scattering processes in the expanding universe. Since we are considering small effects on CMB and abundance of elements, results for any general neutrino spectrum can be obtained by linear superposition of the monochromatic results. We will calculate the constraints on the fraction of decaying dark matter and the resulting N_{eff} , obtained from CMB spectral distortions and abundance of BBN elements, as a function of dark matter decay lifetime or the redshift of energy injection.

2 Evolution of neutrino cascade in the expanding universe

We evolve the injected neutrino distribution in the expanding universe as they interact with the background particles and follow the subsequent particle cascade. We consider neutrino-nucleon scattering and pair production on background neutrino (antineutrinos) to produce electron-positron pairs and quark-gluon pairs. The comparison of the collision rates of these scattering processes with the Hubble rate is shown in Fig. 1 at two redshifts. The cross-section for neutrino-nucleon or neutrino-electron scattering is proportional to the square of center of mass energy which is proportional to the mass of the target particle in the energy range of interest. Therefore, scattering on electrons is negligible compared to nucleons [19]. The difference between the cross-sections for inelastic scattering of high energy neutrinos and anti-neutrinos with nucleons is negligible (See Eq. 14 of [17]). There is no difference between pair-production of standard model particles from high energy neutrinos or anti-neutrinos by annihilation with the background anti-neutrinos or neutrinos respectively since in the center of mass frame they are indistinguishable. The cross-section of neutrinos with the nucleons can be parameterized as a broken power law [17]. The break in the power law

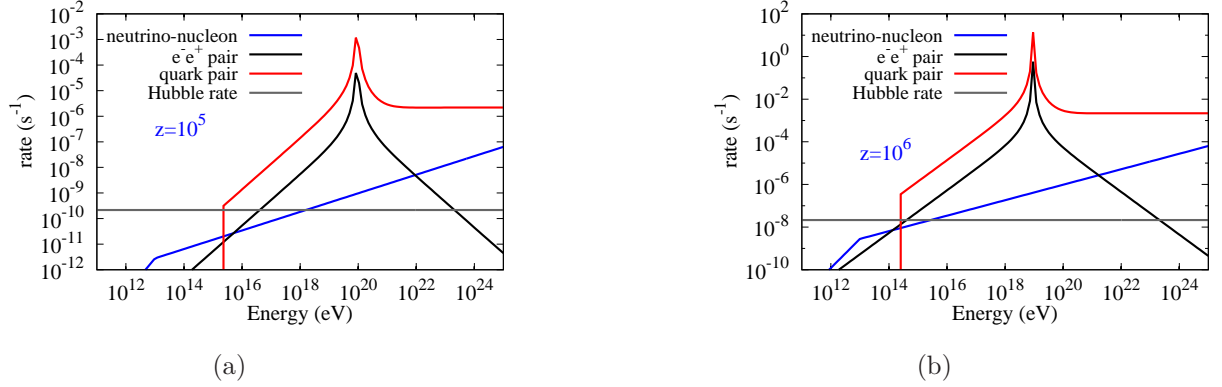


Figure 1: Collision rates of neutrinos or antineutrinos as a function of incident neutrino or antineutrino energy at (a) $z = 10^5$ (b) $z = 10^6$. The peak corresponds to the energy of the incident neutrino such that the center of mass energy for annihilation with background neutrino or anti-neutrino is equal to the Z-boson mass.

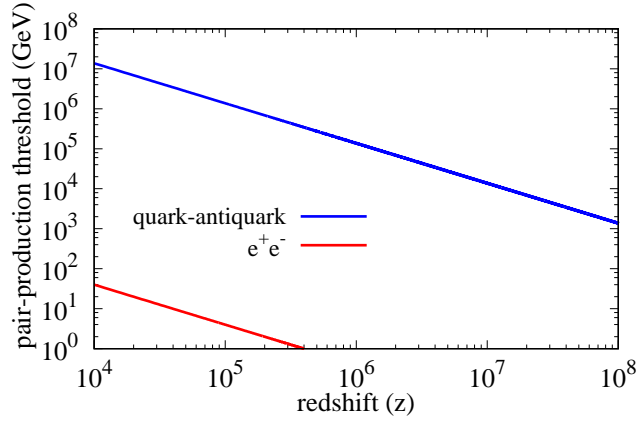


Figure 2: Threshold energy of injected neutrinos (anti-neutrinos) to pair-produce quark-antiquark and electron-positron on annihilation with the background anti-neutrinos (neutrinos).

is due to the increasing importance of scattering with the sea quarks as compared to the valence quarks inside the nucleons. The fraction of neutrino's initial energy retained by the neutrino is parameterized as the inelasticity parameter (see Table 1 and 2 of [17]). This can vary from 50 percent for 10 GeV neutrinos to 20 percent for 10^{12} GeV neutrinos. If the energy of the incident neutrinos is high enough, they can pair produce standard model particles on annihilation with the background anti-neutrinos. The interaction can have both neutral and charged current contribution [20, 21]. The peak in Fig. 1 is the energy of

the incident neutrino such that the center of mass energy for neutrino-antineutrino collision is equal to the Z-boson mass. Beyond this energy, the contribution of neutral current to total cross-section dies away while the contribution of the charged current process dominates the total cross-section [21]. We consider all quarks and gluons to have a mass threshold of 300 MeV, which is the kinematical mass of up and down quarks [55, 56], above which the quarks and gluons are freely emitted. The cross-section for quark pair production is more than an order of magnitude higher compared to e^-e^+ pair production due to more degrees of freedom of quarks and gluons [20]. Therefore, beyond the incident neutrino energy at which quark pair production starts (center of mass energy ≈ 300 MeV), it is the most dominant process. The charged current contribution, important only at high energies, to e^-e^+ pair production channel, is therefore not important and we neglect it. In Fig. 2, we plot the threshold energy of injected neutrinos/anti-neutrinos for pair-production of quark-antiquark and electron-positron pairs by annihilation with background antineutrinos/neutrinos.

The quarks after hadronization produce pions which decay to secondary electrons, positrons, photons, neutrinos, and stable hadrons. The authors in [41] have provided spectra of these decay products from injection of any standard model particle with center of mass energy in the range 5 GeV- 10^6 GeV. This center of mass energy can be translated to lab energy of incident neutrino as $E_\nu = \frac{1}{4}s_{\text{CM}}/E_{\bar{\nu}}$, where s_{CM} is the square of center of mass energy and $E_{\bar{\nu}}$ is the energy of background anti-neutrinos. The energy of background neutrinos and anti-neutrinos at $z \sim 10^8$ is 20 keV. Therefore, the result of [41] can be used for very high energy incident neutrinos upto energy of $E_\nu = 10^{17}$ GeV in the cosmological setup. While the spectrum provided in [41] is in the center of mass (CM) frame, we have to boost it to the CMB frame. For this, we assume the distribution of secondary electromagnetic particles and neutrinos in the center of mass frame to be spherically symmetric. The square of center of mass energy for collisions of injected high energy neutrino with energy E_ν with background anti-neutrino is given by,

$$s_{\text{CM}} = 4.0 \times E_\nu \times \left(\frac{4}{11}\right)^{1/3} k_B T_{\text{CMB}}, \quad (2.1)$$

where k_B is the Boltzmann constant and $T_{\text{CMB}} = 2.725(1+z)\text{K}$ is the CMB temperature. We assume that the background neutrinos and anti-neutrinos to have energy $\approx k_B T_\nu \approx \left(\frac{4}{11}\right)^{1/3} k_B T_{\text{CMB}}$, where T_ν is the temperature of neutrinos in standard ΛCDM cosmology. If the neutrinos are their own antiparticles (Majorana) the number density of each flavor i of neutrino at redshift z is given by,

$$n_\nu^i(z) \equiv n_{\bar{\nu}}^i(z) = \left(\frac{3}{4}\right) \times \left(\frac{4}{11}\right) n_\gamma(z), \quad (2.2)$$

where n_γ is the total number density of CMB photons at redshift z . The background number density is important only for the annihilation of injected neutrinos/antineutrinos with the cosmic neutrino background (CNB) particles. For Dirac particles, the number density of the target background neutrinos and anti-neutrinos gets halved. However, whenever the $\nu\bar{\nu}$ annihilation is important compared to the other collision processes, it is also much faster compared to the Hubble rate (Fig. 1). This means that almost all injected neutrinos would

annihilate in this regime and a factor of 2 change in the number density of the annihilation targets due to neutrinos being Dirac or Majorana fermions has a negligible effect on the results. Our results are therefore valid irrespective of whether neutrinos are Dirac or Majorana fermions.

The Lorentz factor of center of mass frame is given by, $\gamma_{\text{CM}} = \frac{E_\nu}{\sqrt{s_{\text{CM}}}}$. A monochromatic energy source with spherically symmetric distribution in the CM frame is boosted to a box distribution in the lab frame or Friedmann metric/background frame i.e.,

$$\frac{dN}{dE} \propto \Theta(E - E_-)\Theta(E_+ - E), \quad (2.3)$$

where N is the comoving number density of particles, $\Theta(x)$ is the Heaviside step function such that $\Theta(x) = 1$ for $x > 0$ and $\Theta(x) = 0$ for $x < 0$, $E_\pm = \frac{\gamma_{\text{CM}}}{2}E(1 \pm \beta_{\text{CM}})$, β_{CM} is the boost factor, and E is the energy of secondary neutrinos in the center of mass frame. We superpose the lab spectrum for all secondary neutrinos produced in quark hadronization to get the full spectrum. Although the secondary neutrinos will have lower energies compared to the original injected neutrinos, some secondary neutrinos in the high energy tail of the spectrum can still pair-produce. Low energy neutrinos mostly redshift while depositing a small fraction of their energy due to inelastic scattering with nucleons. The electromagnetic energy deposited at $z \gtrsim 2 \times 10^5$ thermalizes to a Bose-Einstein spectrum and μ -type distortion is a good approximation [29]. In particular, in this regime of thermal spectral distortions, only total injected electromagnetic energy is required and the actual spectrum of injected electromagnetic particles is not needed. However, we need the spectrum of electromagnetic particles in order to calculate the photo-dissociation of light elements produced in the BBN since there is a threshold energy below which electromagnetic particles are unable to photo-dissociate the elements. Therefore, we calculate the spectra of electromagnetic particles as well. These secondary electromagnetic particles can lead to electromagnetic cascades which themselves have to be evolved in the expanding universe [29], but in this work we ignore this. Instead, we assume that any electromagnetic energy injected at a particular timestep is deposited at that redshift as heat to the background electrons giving rise to CMB spectral distortion or goes into photo-dissociation of nuclei. We, therefore, calculate the photo-dissociation of elements only for the initial injected photons in the on-the-spot approximation, which is a good approximation at $z \gtrsim 10^5$. We compare the on-the-spot approximation with the full calculation in Appendix B.

A fraction of neutrinos, with energy greater than the mass of W, Z bosons, can decay to these particles which after hadronic and leptonic cascade produce stable standard model particles on timescales much shorter than the Hubble time [16]. The particle spectrum with electroweak shower can be computed in **PYTHIA** [56] and has been included in the data provided by [41]. Thus, neutrinos (anti-neutrinos) with energy ~ 100 GeV can still give rise to reasonable spectral distortion and BBN signature, even though they can not pair-produce quarks on the background anti-neutrinos (neutrinos).

To evolve the particle spectrum, we divide the energy $\sim \text{eV}-10^{21} \text{ eV}$ in 300 log

spaced dimensionless energy bins in dimensionless energy variable $x = \frac{E}{k_B T_{\text{CMB}}}$, where k_B is the Boltzmann constant and T_{CMB} is the CMB temperature. Using dimensionless energy variable x takes care of redshifting of energy due to expansion of the universe implicitly. A particle only redshifting away its energy will stay in the same x bin. The details of our calculation of particle cascade are described in Appendix A.

3 Dark matter decaying into neutrinos and the resulting N_{eff}

We consider high energy monochromatic neutrino injection from decay of long-lived unstable particles in the dark sector. The energy injection from dark matter decay can be parameterized by,

$$\frac{d\rho}{dt} = \frac{f_X}{\tau_X} \rho_c c^2 (1+z)^3 e^{-(t/\tau_X)}, \quad (3.1)$$

where ρ is the injected energy density, f_X is the fraction of decaying dark matter compared to total dark matter, ρ_c is the energy density of total dark matter, c is the speed of light, τ_X is the dark matter lifetime with corresponding redshift denoted as z_X . The relative change in the CMB energy density due to electromagnetic energy injection in a redshift bin $|\Delta z|$ at z is given by,

$$\Delta\epsilon(z) = \frac{\Delta\rho_{\text{CMB}}(z)}{\rho_{\text{CMB}}(z)}, \quad (3.2)$$

where $\Delta\rho_{\text{CMB}}$ is the injected electromagnetic energy density and ρ_{CMB} is the standard model CMB energy density given by $\rho_{\text{CMB}} = 0.26(1+z)^4 \text{ eV/cm}^3$. The total fractional change of CMB energy density at a particular redshift z is given by integration of fractional change of CMB energy density from starting redshift of energy injection (z_{st}) upto that redshift i.e.,

$$\epsilon(z) = \int_{z_{st}}^z \frac{d[\Delta\rho_{\text{CMB}}(z_{inj})/\rho_{\text{CMB}}(z_{inj})]}{dz_{inj}} dz_{inj}. \quad (3.3)$$

The fractional change of CMB energy density which shows up as spectral distortion in the CMB is given by,

$$\epsilon_{SD}(z) = \int_{z_{st}}^z \frac{d[\Delta\rho_{\text{CMB}}(z_{inj})/\rho_{\text{CMB}}(z_{inj})]}{dz_{inj}} e^{-\tau(z_{inj})} dz_{inj}, \quad (3.4)$$

where $\tau(z_{inj})$ is the μ -visibility function, which is given by $\tau(z_{inj}) \approx e^{-(z_{inj}/z_\mu)^{2.5}}$ with $z_\mu = 2 \times 10^6$ [23, 31, 32]. The amplitude of μ -type distortion from energy injection can be written as,

$$\mu = 1.4 \int_{z_{st}}^{z_t} \frac{d[\Delta\rho_{\text{CMB}}(z_{inj})/\rho_{\text{CMB}}(z_{inj})]}{dz_{inj}} e^{-\tau(z_{inj})} dz_{inj}, \quad (3.5)$$

where $z_t \approx 2 \times 10^5$. At $z \lesssim z_t$, μ -type distortion is no longer a good approximation and we should take into account the actual spectrum of spectral distortions [30] when calculating

constraints. The energy density of relativistic freestreaming particles is parameterized by N_{eff} such that their energy density well after electron-positron annihilation is given by

$$\rho_\nu = N_{\text{eff}} \left(\frac{7}{8} \right) \left(\frac{4}{11} \right)^{4/3} \rho_{\text{CMB}}, \quad (3.6)$$

where ρ_ν is the energy density of neutrinos in ΛCDM cosmology and $N_{\text{eff}} = 3.046$. In case of electromagnetic energy injection, ρ_{CMB} will increase compared to ρ_ν and N_{eff} will be smaller compared to the ΛCDM model. On the other hand, if we inject neutrinos, the N_{eff} will be expected to increase if the energy of neutrinos \lesssim GeV. For the case of ultra-high energy neutrinos that we are interested in, with energy $\gtrsim 100$ GeV, a fraction of initial energy injected in neutrinos will be lost to electromagnetic particles and end up in increasing the energy density of CMB. Depending upon what fraction of initial neutrino energy is dissipated electromagnetically and what fraction remains with secondary neutrinos, N_{eff} can either increase or decrease.¹ With energy injection, the expression for modified N_{eff} is given by,

$$N_{\text{eff}}^* = \frac{\rho_\nu^*}{\left(\frac{7}{8} \right) \left(\frac{4}{11} \right)^{4/3} \rho_{\text{CMB}}^*}, \quad (3.7)$$

where $\rho_\nu^* = \rho_\nu + \Delta\rho_\nu$, $\rho_{\text{CMB}}^* = \rho_{\text{CMB}} + \Delta\rho_{\text{CMB}}$, where $\Delta\rho_\nu$ and $\Delta\rho_{\text{CMB}}$ are the change in neutrino and CMB energy density due to energy injection respectively. For small energy injections ($\frac{\Delta\rho_{\text{CMB}}}{\rho_{\text{CMB}}}, \frac{\Delta\rho_\nu}{\rho_\nu} \ll 1$), the expression for N_{eff}^* can be written as,

$$N_{\text{eff}}^* = N_{\text{eff}} + N_{\text{eff}} \left(\frac{\Delta\rho_\nu}{\rho_\nu} - \frac{\Delta\rho_{\text{CMB}}}{\rho_{\text{CMB}}} \right), \quad (3.8)$$

and the deviation in free streaming relativistic degrees of freedom $\Delta N_{\text{eff}} = N_{\text{eff}}^* - N_{\text{eff}}$ is given by,

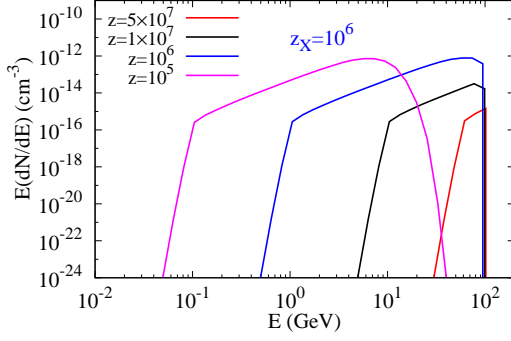
$$\Delta N_{\text{eff}} = N_{\text{eff}} \left(\frac{\Delta\rho_\nu}{\rho_\nu} - \frac{\Delta\rho_{\text{CMB}}}{\rho_{\text{CMB}}} \right). \quad (3.9)$$

Total $\Delta N_{\text{eff}}(z)$ at z from energy injection at all higher redshifts can be calculated by summing up contribution from all previous redshift bins as,

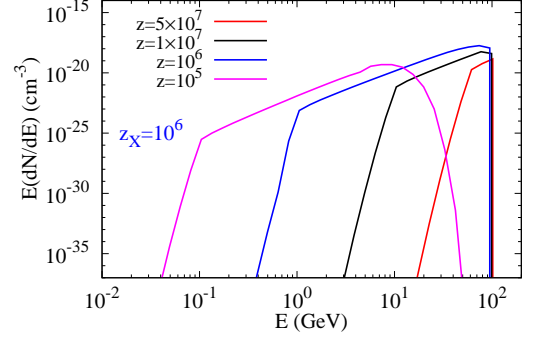
$$\Delta N_{\text{eff}}(z) = \int_{z_{\text{st}}}^z \frac{d(\Delta N_{\text{eff}})}{dz_{\text{inj}}} dz_{\text{inj}}. \quad (3.10)$$

The electromagnetic energy from high energy neutrinos contribute to $\Delta\rho_{\text{CMB}}$ while the surviving primary as well as secondary neutrinos contribute to $\Delta\rho_\nu$. The electromagnetic energy released before $z = 2 \times 10^6$ thermalizes creating a temperature shift of the CMB while energy deposited at later redshifts create a $n\text{tr}$ or μ distortion. We note that even when electromagnetic energy injection does not create spectral distortions at $z \gtrsim 2 \times 10^6$, it still changes N_{eff} and contributes to ΔN_{eff} i.e. both temperature shift and distortion in the CMB contribute to $\Delta\rho_{\text{CMB}}$.

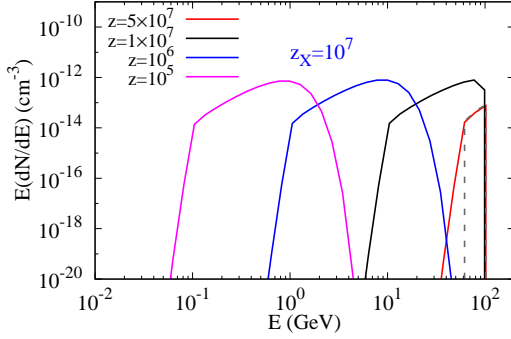
In Fig. 3 and 4, we plot the instantaneous neutrino and electromagnetic spectrum



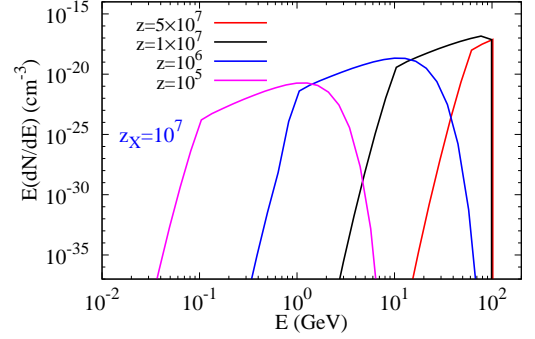
(a) neutrino



(b) Photon/electron



(c) neutrino

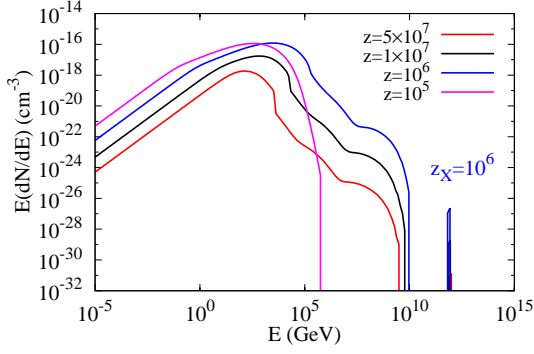


(d) Photon/electron

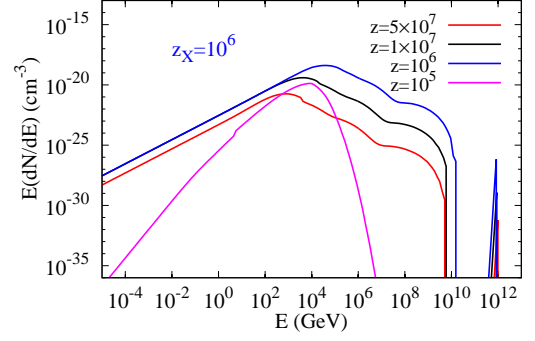
Figure 3: Instantaneous spectrum of neutrinos and electromagnetic particles $\frac{dN}{d\ln E}$ (comoving energy density per unit log energy) at different redshifts for 100 GeV initial neutrino injection from dark matter decay with lifetime as denoted in the figure. The electromagnetic spectrum is not evolved in redshift but obtained from instantaneous neutrino spectrum at that redshift. The dotted line in 3c is obtained by neglecting neutrino-nucleon scattering. We have assumed $f_X = 0.1$ for this figure.

of injected primary as well as secondary particles for dark matter decay with different z_X for initial injection of 100 GeV and 10^{12} GeV neutrinos. For 10^{12} GeV neutrino injection, there are surviving neutrinos at 10^{12} GeV as well as secondary neutrinos after quark-antiquark pair production which have significantly lower energy. For 100 GeV neutrinos, there is no quark-antiquark pair-production and we have a smooth and continuous spectrum from surviving neutrinos. The instantaneous electromagnetic spectrum is obtained from energy release of instantaneous neutrino spectrum after collision with background particles. The electromagnetic particles as well as neutrinos are produced after hadronization and electromagnetic energy is released from neutrino-nucleon scattering which is a function of neutrino spectrum. Therefore, the spectrum of electromagnetic particles is qualitatively similar to neutrinos. In Fig. 3c,

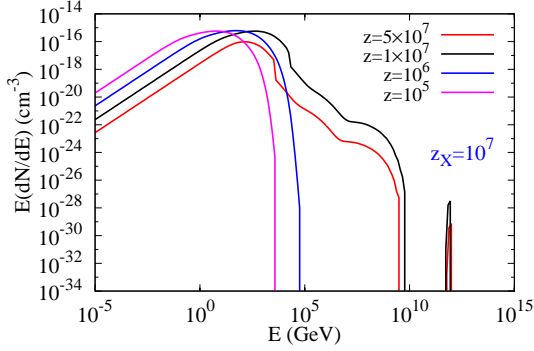
¹A related discussion can be found in Sec. 6.1 of [57] and [58].



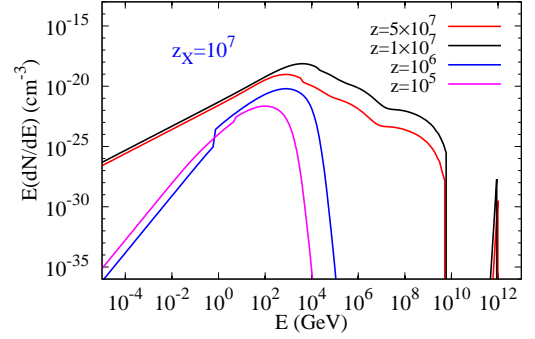
(a) neutrino



(b) Photon/electron



(c) neutrino



(d) Photon/electron

Figure 4: Instantaneous spectrum of injected neutrinos and electromagnetic particles $\frac{dN}{d\ln E}$ (comoving number density per unit log energy) at different redshifts for 10^{12} GeV initial neutrino injection from dark matter decay with lifetime as denoted in the figure. We have assumed $f_X = 0.1$ for this figure.

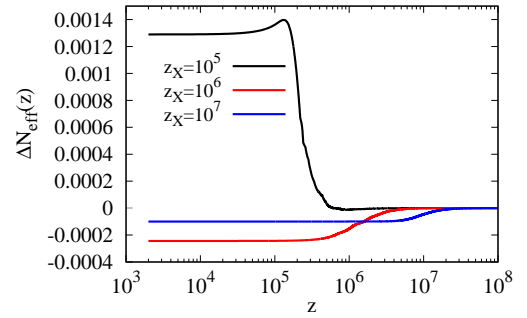
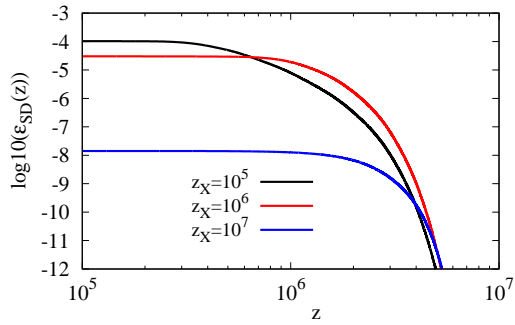


Figure 5: (a) $\epsilon_{SD}(z)$ and (b) ΔN_{eff} from injection of 10^6 GeV neutrinos as a function of redshift with $f_X = 10^{-4}$ for different z_X .

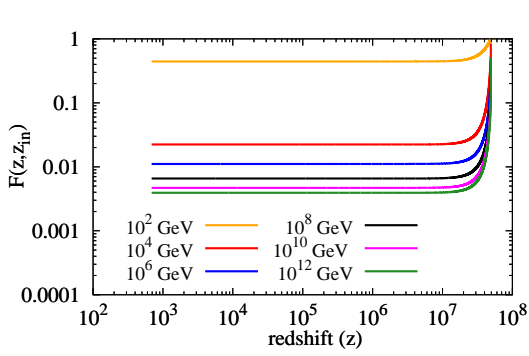
the dotted curve is calculated ignoring neutrino-nucleon scattering. With neutrino-nucleon scattering taken into account, the spectrum spreads out a little as neutrinos lose energy.

In Fig. 5, we show the evolution of $\epsilon_{SD}(z)$ and $\Delta N_{\text{eff}}(z)$ by energy injection from dark matter decay (with $f_X = 10^{-1}$) to 10^6 GeV neutrinos for a few values of z_X . The starting redshift for calculation (z_{st}) is chosen to be 10^8 . At higher redshifts, the probability for neutrinos to release their energy as electromagnetic energy is higher because the background neutrinos and anti-neutrinos are at higher temperature, and hence, there is a higher probability of electron-positron and quark-anti-quark pair production. There can be multiple cycles of pair productions as high energy tails of secondary neutrinos can again pair-produce on background anti-neutrinos and vice versa. Also, there is a higher probability of neutrino-nucleons inelastic scattering as the density of nucleons (or baryons) is higher at higher redshifts. Therefore, contribution to $\Delta N_{\text{eff}}(z)$ from fractional change in CMB energy density dominates and $\Delta N_{\text{eff}}(z)$ is negative. At lower redshifts, extra neutrino energy density contribution to $\Delta N_{\text{eff}}(z)$ starts to dominate as there is an increase in the probability for neutrinos to survive. Both $\epsilon_{SD}(z)$ and magnitude of $\Delta N_{\text{eff}}(z)$ decrease with increasing z_X as energy release from dark matter decay is proportional to $(1+z)^3$ while the background neutrino and CMB energy density $\propto (1+z)^4$. Once the dark matter has completely decayed, there is no more energy injection and $\epsilon_{SD}(z)$ and $\Delta N_{\text{eff}}(z)$ become constant as interaction of surviving low energy neutrinos with background particles becomes negligible. The decrease in magnitude of $\epsilon_{SD}(z)$ is more drastic compared to $\Delta N_{\text{eff}}(z)$ with increasing redshift due to the μ -visibility function. We have assumed that the amount of energy injection with respect to the CMB is small. This assumption is not valid at high redshifts since at $z > 2 \times 10^6$ energy injection of order ρ_{CMB} is also allowed by the COBE data because of the exponential suppression of spectral distortions. A recent study [57] has relaxed this assumption at least for one-time energy injection. For continuous energy injection, we must calculate on case-by-case basis. We will, however, continue to use the simple analytic expression for the μ -visibility function since we are mostly interested in small spectral distortions created by surviving neutrinos at $z \lesssim 2 \times 10^6$. The increase in the efficiency of photon production processes such as bremsstrahlung and double Compton scattering results in any electromagnetic energy injection to thermalize, creating a Planck spectrum with higher temperature and exponential decrease in the magnitude of the CMB spectral distortion at $z \gtrsim 2 \times 10^6$. There is no such restriction for neutrinos since they interact weakly, deposit their energy slowly, and can survive for a long time. In particular, neutrinos injected at $z \gtrsim 2 \times 10^6$ can survive until $z \lesssim 2 \times 10^6$ and deposit some of their energy in electromagnetic particles at a time when the CMB spectral distortions can survive.

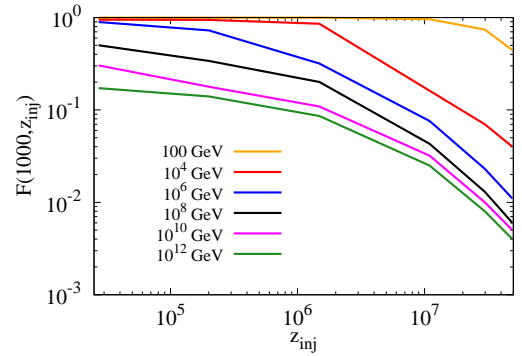
In Fig. 6a, we plot the fraction of injected energy surviving as neutrinos ($F(z, z_{inj})$) at $z < z_{inj}$ for one-time energy injection at z_{inj} . The expression for $F(z, z_{inj})$ is given as,

$$F(z, z_{inj}) = \frac{\Delta \rho_\nu(z)}{\Delta \rho_\nu(z_{inj})}, \quad (3.11)$$

where $\Delta \rho_\nu(z)$ is the surviving neutrino energy density at z and $\Delta \rho_\nu(z_{inj})$ is the injected neutrino energy density at z_{inj} . With increasing energy of injected neutrinos, $F(z, z_{inj})$ decreases as it



(a) Fraction of surviving neutrino energy $F(z, z_{inj})$ as a function of redshift for one-time energy injection at $z_{inj}=4 \times 10^7$.



(b) $F(1000, z_{inj})$ for one-time energy injection at z_{inj} for different values of initial neutrino energy.

Figure 6: $F(1000, z_{inj})$ for neutrinos as a function of neutrino energy and injection redshift.

is more likely for neutrinos to lose their energy after multiple pair-production cycles of quark-antiquarks. This shows up a vertical fall in $F(z, z_{inj})$ as rate of quark-antiquark pair production is much faster than the Hubble rate. In Fig. 6b, we plot the extra energy in neutrinos surviving at $z = 1000$, $F(1000, z_{inj})$, as a function of z_{inj} . The surviving extra energy in neutrinos at $z = 1000$ decreases with increase in neutrino energy as well as injection redshifts. For any z_{inj} , the efficiency of energy deposition by neutrinos decreases with decreasing redshift as the neutrino energy redshifts and the number density of target particles for collisions also decreases. Thus $F(z, z_{inj})$ approaches an asymptotic constant value for $z \ll z_{inj}$. In particular for $z_{inj} \gg 1000$, we expect $F(z, z_{inj})$ as well as ΔN_{eff} to be frozen by $z \approx 1000$.

4 CMB spectral distortion constraints

We now use COBE-FIRAS [42–44] data to constrain the high energy neutrino injection. For $z_X > 3 \times 10^5$, μ -type distortion is a good approximation² and we use the 95 percent μ -distortion limit of COBE-FIRAS, $\mu < 9 \times 10^{-5}$. For $z_X < 3 \times 10^5$, μ -type distortion (or even i or y type distortions) is no longer a good approximation and we should use the actual spectrum of spectral distortions (ntr -type distortions) [30]. The constraints for ntr -type distortions were derived by fitting the ntr -type CMB spectral distortions to the COBE-FIRAS data in [30] where it was also shown that when the energy of injected particles is $\gtrsim 1\text{GeV}$, the CMB spectral distortion becomes independent of the energy of the injected particles as well as whether the particle is an electron or photon. We will use these $\gtrsim 1\text{GeV}$ ntr -type spectral distortion constraints. This is motivated from the fact that photons/electrons produced from neutrino/anti-neutrino pair-production have $\gtrsim \text{GeV}$ energy (Fig. 3 and 4).

²Note that for decay redshift z_X significant energy injection will continue for sometime even at $z < z_X$.

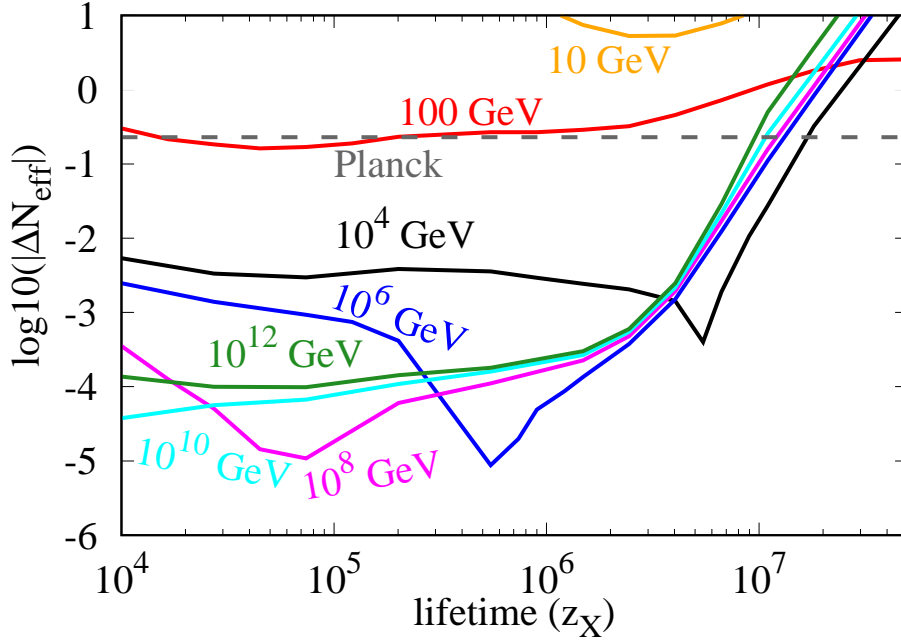


Figure 7: $2\text{-}\sigma$ Constraint of $|\Delta N_{\text{eff}}|$ from CMB spectral distortions (μ -type and ntr -type) using COBE-FIRAS data [44] as a function of dark matter lifetime for different values of monochromatic neutrino energy. *Planck* constraint [1] is shown as dashed line.

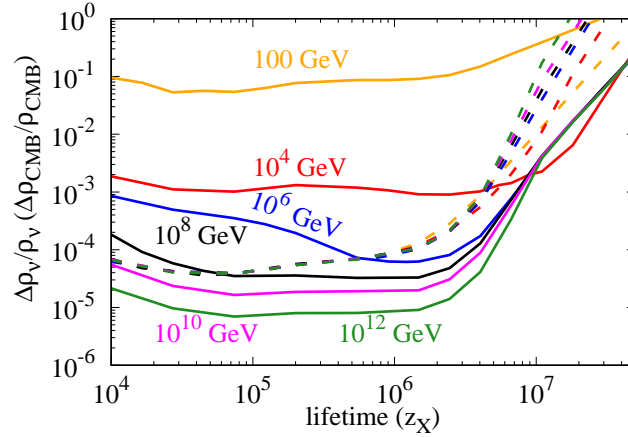


Figure 8: The fractional changes in neutrino energy density $\frac{\Delta\rho_\nu}{\rho_\nu}$ (solid lines) and CMB energy density $\frac{\Delta\rho_{\text{CMB}}}{\rho_{\text{CMB}}}$ (dashed lines) contributing to $|\Delta N_{\text{eff}}|$ constraints plotted in Fig. 7.

We define the correction factor ($C(z_X)$), a function of z_X , as the ratio of actual constraint on the amount of energy injected using the $\gtrsim 1\text{ GeV}$ ntr -distortion to the constraint we would

lifetime (z_X)	correction factor (C)
5×10^3	1.99
6×10^3	1.66
8×10^3	1.21
1×10^4	1.06
2×10^4	0.69
3×10^4	0.63
4×10^4	0.60
5×10^4	0.59
6×10^4	0.59
7×10^4	0.60
8×10^4	0.63
9×10^4	0.64
1×10^5	0.67
2×10^5	0.85
3×10^5	0.97
4×10^5	1.009
5×10^5	1.005

Table 1: Correction factor for COBE-FIRAS data [44] to convert the constraint assuming all energy goes into μ -type distortions to the constraint for $\gtrsim 1$ GeV ntr -type distortions.

obtain if we assumed that the energy for $z_X < 3 \times 10^5$ also created μ -type distortion. Thus a $C > 1$ means that the actual constraints are weaker compared to what we would have inferred if we assumed that all energy went into μ -type distortions. We give this correction factor in Table 1 calculated using ntr -type distortions constraints of [30]. Note that this correction factor depends on the experiment, in particular the sensitivity of different frequency channels of the experiment, and is calculated for COBE-FIRAS data in Table 1. We thus first calculate the constraints by assuming that all electromagnetic energy goes into μ -type distortion giving $\mu = 1.4\epsilon_{SD}$ and then apply the correction factor to get the actual constraint. The correction factor at low redshifts is greater than 1 due to reduction of spectral intensity of distortion in the CMB bands as relativistic electrons boost the CMB photons to high energy tail of the CMB spectrum and significant amount of energy ends up out of the CMB band. Therefore, higher energy injection is allowed compared to μ -type distortion. At higher redshifts, the distorted CMB spectrum partially thermalizes to i -type distortion [27, 28], for which energy injection constraint can be stronger compared to μ -distortion [30]. The correction factor approaches unity at $z_X \gtrsim 3 \times 10^5$.

In Fig. 7, we show $2\text{-}\sigma$ constraints from COBE-FIRAS on $|\Delta N_{\text{eff}}(1000)|$ (from now on, we assume $\Delta N_{\text{eff}}(z)$ to be computed at $z = 1000$ and we drop the functional dependence on z from now on) as a function of z_X for different values of initial neutrino energy, taking into account

the correction for the *ntr*-type distortions. We also show *Planck* constraint [1] as dashed line, $|\Delta N_{\text{eff}}| \sim 0.3$ at $2\text{-}\sigma$. For 10 GeV neutrinos, the constraints obtained from CMB spectral distortions are very weak. For neutrinos with energy $\gtrsim 100$ GeV, the spectral distortion constraints become stronger than *Planck*. For 100 GeV neutrinos, the fraction of energy lost to electromagnetic particles through electroweak showers can be 0.1 percent. The fraction of energy lost to electromagnetic particles increases with energy and saturates to about 20 percent at ultra high energies. Since the surviving neutrino energy density dominates the increase in CMB energy density for 100 GeV case, ΔN_{eff} is positive in this case. The kink feature in $10^4 - 10^8$ GeV neutrinos is due to the change in the sign of ΔN_{eff} as discussed before. The individual contributions, $\frac{\Delta\rho_\nu}{\rho_\nu}$ and $\frac{\Delta\rho_{\text{CMB}}}{\rho_{\text{CMB}}}$ to ΔN_{eff} are plotted in Fig. 8 and the kink feature in ΔN_{eff} constraints can be seen in Fig. 8 as the crossing of $\frac{\Delta\rho_\nu}{\rho_\nu}$ and $\frac{\Delta\rho_{\text{CMB}}}{\rho_{\text{CMB}}}$ curves. The location of kink or crossover between $\frac{\Delta\rho_\nu}{\rho_\nu}$ and $\frac{\Delta\rho_{\text{CMB}}}{\rho_{\text{CMB}}}$ is a function of neutrino energy. The curves $\frac{\Delta\rho_{\text{CMB}}}{\rho_{\text{CMB}}}$ for all values of neutrino energy fall on top of each other at $z_X \lesssim 2 \times 10^6$ in Fig. 8 as most of electromagnetic energy deposited to the CMB shows up as spectral distortion and is constrained to be of the order 10^{-4} by COBE-FIRAS [43, 44]. For $z_X \gtrsim 2 \times 10^6$, the electromagnetic energy deposited at $z \gtrsim 2 \times 10^6$ does not produce a spectral distortion and is, therefore, not constrained by the data. The $\frac{\Delta\rho_{\text{CMB}}}{\rho_{\text{CMB}}}$ curves in Fig. 8 diverge from each other as the amount of electromagnetic energy deposited in the CMB at $z \lesssim 2 \times 10^6$ for neutrino energy injection at $z \gtrsim 2 \times 10^6$, and therefore the constraint from CMB spectral distortions, is a function of neutrino energy. Neutrinos injected at high redshifts will rapidly pair produce, giving rise to a broad low energy neutrino spectrum below the pair production threshold erasing any information of original neutrino energy. This makes the $\frac{\Delta\rho_\nu}{\rho_\nu}$ curves converge to each other for high initial neutrino energies. With increase in neutrino energy, the threshold of pair production of quark-antiquark pairs (also true for electron-positron pairs but is unimportant as pair production rate of e^-e^+ is much slower compared to the Hubble rate (Fig. 1)) occurs at lower redshifts. The higher energy ($\gtrsim 10^6$ GeV) cases are all pair production dominated at $z \lesssim 2 \times 10^6$. Therefore, ΔN_{eff} is negative for all redshifts for these cases. For pair production to e^-e^+ , all of the neutrino energy and for quarks almost 50 percent of the neutrino energy is released as electromagnetic particles. The secondary neutrinos can themselves pair produce again and again, the probability of which increases with increase in incident neutrino energy. This increases the probability of electromagnetic energy release which reduces the energy density in surviving neutrinos or $\frac{\Delta\rho_\nu}{\rho_\nu}$.

In Fig. 9, we compare the constraints on ΔN_{eff} including only quark pair production process with the case when we include all scattering processes i.e. including quark-antiquark, electron-positron pair production, and neutrino-nucleon inelastic scattering. From Fig. 1, we can see that the quark pair production rate is much faster than the Hubble rate. Therefore, electromagnetic release from neutrinos is instantaneous just like pure electromagnetic energy injection. Hence, the constraints with only quark-antiquark pair production track the μ -visibility curve. The low energy surviving neutrinos below the quark pair production threshold can deposit their energy at much slower rate compared to the Hubble rate. Therefore, with

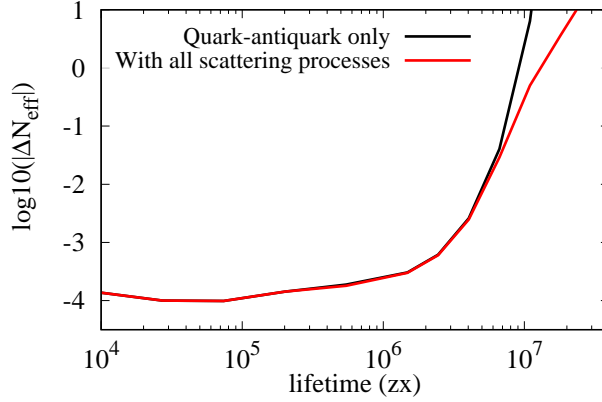


Figure 9: 2- σ Constraints on $|\Delta N_{\text{eff}}|$ from CMB spectral distortions including only quark-antiquark pair production and including quark-antiquark, electron-positron pair production and neutrino-nucleon scattering. Energy of injected neutrino is 10^{12} GeV.

these additional processes, we can probe higher redshifts as shown in Fig. 9. At $z \lesssim 2 \times 10^6$, we can ignore the neutrino-nucleon scattering and e^-e^+ pair production, since quark pair production drives the ΔN_{eff} constraints as long as the energy of injected neutrinos exceeds the pair production threshold.

5 Constraints from abundance of light elements

Elements	theoretical value(1σ)	observational value(1σ)
$n_{2\text{H}}/n_{\text{H}}$	$(2.58 \pm 0.13) \times 10^{-5}$ [59]	$(2.53 \pm 0.04) \times 10^{-5}$ [59]
Y_p	0.24709 ± 0.00025 [59]	0.2449 ± 0.0040 [60]
$n_{3\text{He}}/n_{\text{H}}$	$(10.039 \pm 0.090) \times 10^{-6}$ [59]	1.5×10^{-5} (2σ upper limit) [61]

Table 2: Theoretical and observational bounds on light element abundance that are used in this work for deuterium ($n_{2\text{H}}$) and helium-3 number density ($n_{3\text{He}}$) with respect to hydrogen number density (n_{H}). Helium-3 and Deuterium over-production provide stronger constraints compared to change in Helium-4 (^4He) mass fraction (Y_p), where Y_p is the ratio of helium mass density to the total mass density of hydrogen and helium.

High energy photons, in the electromagnetic shower produced by injected neutrinos above helium and deuterium photo-dissociation thresholds (19.81 and 2.2 MeV respectively), can dissociate helium-4 producing helium-3 and deuterium or destroy deuterium, thus changing

the primordial abundance of these light nuclei. We can use the theoretical and observational bounds on the abundance of helium-3 and deuterium to constrain the energy injection scenarios. The bounds on abundance used in this calculation are given in Table 2 and the procedure to obtain the constraints is detailed in [40]. To obtain BBN constraints from electromagnetic energy injection, we have to evolve the electromagnetic cascade along with the abundance of primordial elements, which are being created and destroyed, in the expanding universe [35–40]. Photons are evolved with Compton scattering, e^-e^+ pair production on the CMB photons and background electrons and nuclei, photon-photon elastic scattering, and photo-dissociation of elements. There is a competition between photodissociation and other processes which degrade the injected photon energy. When the energy of degraded photons fall below ~ 20 MeV, there is no photo-dissociation of helium-4 anymore. The constraints obtained from BBN for high energy photons and electrons ($> \text{GeV}$) are essentially universal and do not depend upon the energy of injected photon and electron [35]. This is because high energy photon scattering processes such as e^-e^+ pair production on the CMB and photon-photon elastic scattering are extremely efficient in processing the high energy photons and creating a broad low energy spectrum, irrespective of the energy of the original photon. Recently, it was shown that this may not be true for 10-100 MeV electromagnetic particles and the constraints are non-universal [36, 38–40]. Here, we do a simplified analysis in the on-the-spot approximation which means that all the electromagnetic energy injected at a redshift either creates or destroys elements or degrades to sub-MeV energy at that redshift (see Appendix B for a discussion on comparison of on-the-spot approximation and the full calculation). We also ignore the shape of the electromagnetic spectrum above 2.2 MeV and assume all particles to have energy $\gtrsim \text{GeV}$. This is a good approximation as most of the secondary photon/electron have energy greater than GeV as can be seen in Fig. 3 and 4.

We first tabulate what fraction of a $\sim \text{GeV}$ photon’s or electron’s energy is used up as creation and destruction of primordial elements as a function of redshift. We then use this tabulated data with the electromagnetic energy released from the neutrino cascade to get the change in the primordial nuclear abundance as a function of redshift. We find that the strongest constraints come from creation of helium-3 by destruction of helium-4 as the cross-section for photo-dissociation of helium-4 to helium-3 is an order of magnitude higher compared to dissociation of helium-4 to deuterium. There are however systematic uncertainties in astrophysical observation of helium-3 [37, 62]. Constraints from deuterium destruction are weak due to its low abundance ($\sim 10^{-5}$ times the number density of helium-4) and we do not consider them in this paper.

In Fig. 10 and 11, we plot constraints on ΔN_{eff} allowed by abundance of primordial elements. We see similar patterns as in the case of spectral distortions. The constraints initially get stronger with increasing redshifts. Electrons and positrons in the electromagnetic cascade can boost the CMB photons to higher energy at higher redshifts as the average energy of CMB photons are higher. Thus, more photons are available above the photo-dissociation threshold of helium-4. At still higher redshifts, constraints weaken as the injected photons can efficiently pair produce e^-e^+ on the CMB photons. Once the electron-positron pair production

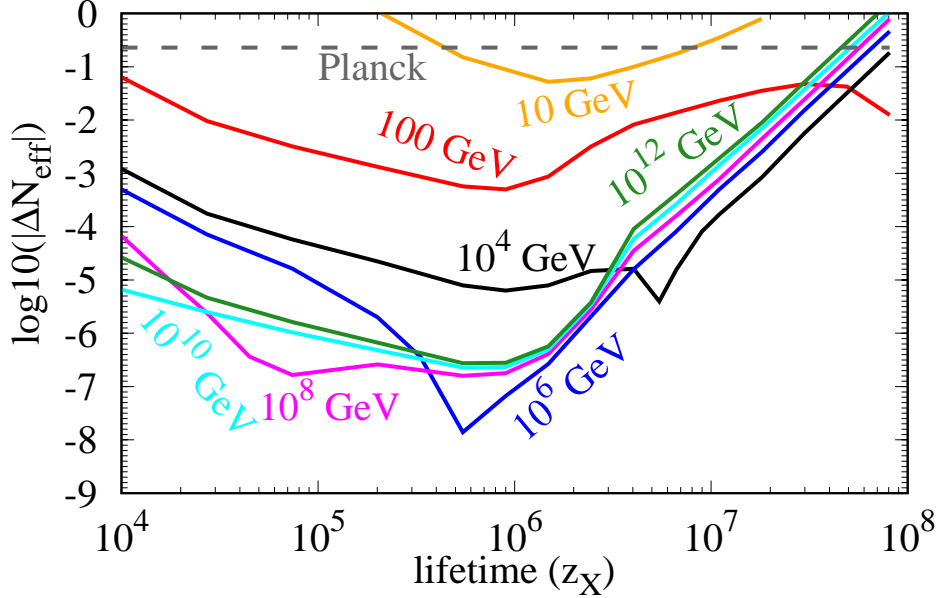


Figure 10: $2\text{-}\sigma$ Constraint of $|\Delta N_{\text{eff}}|$ from change in primordial nuclear abundance from destruction of helium-4 into helium-3 as a function of dark matter lifetime with different monochromatic injected neutrino initial energy.

threshold of energetic photons on the CMB photons is of similar energy as compared to the photo-dissociation threshold of helium-4, the photons are degraded efficiently to sub-MeV energy instead of destroying helium, resulting in weakening of constraints. This can be clearly seen in Fig. 12. With quark pair production only, the constraints weaken much faster as compared to the case when we consider the lower energy scattering processes of neutrinos. The ΔN_{eff} constraints obtained for COBE [44], abundance of light elements, and projection from PIXIE [46] are summarized in Fig. 13. In Fig. 14, we plot the $2\text{-}\sigma$ constraint for decaying dark matter abundance for the neutrino decay channel as a function of its lifetime. Since energy injection from dark matter decay scales with redshift as $(1+z)^3$ while energy density of CMB goes as $(1+z)^4$, constraint on f_X from CMB spectral distortion scales as $(1+z)$ for $z \lesssim 10^6$. The abundance of light elements scales as $(1+z)^3$, therefore, constraints on f_X in this case are flatter with respect to redshift of injection for $z \lesssim 10^6$.

6 Conclusion

In this work, we have obtained constraints on injection of high energy neutrinos in the early universe using dark matter decay as an example and the resulting free streaming degrees of freedom at recombination epoch parameterized by ΔN_{eff} . High energy neutrinos (anti-neutrinos) can deposit a fraction of their energy as electromagnetic energy by pair producing

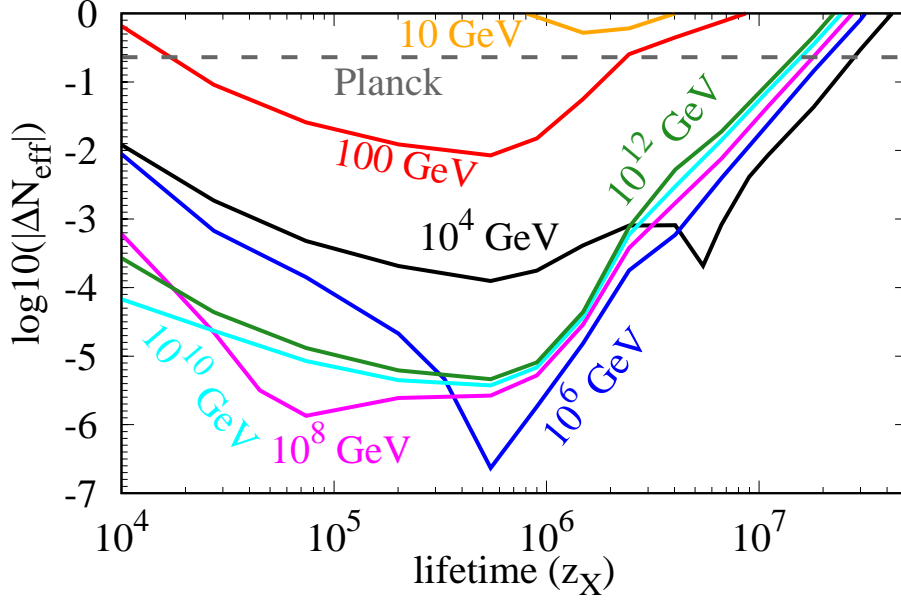


Figure 11: $2\text{-}\sigma$ Constraint on $|\Delta N_{\text{eff}}|$ from change in primordial nuclear abundance of helium-3 by destruction of helium-4 into deuterium as a function of dark matter lifetime with different values of monochromatic injected neutrino initial energy.

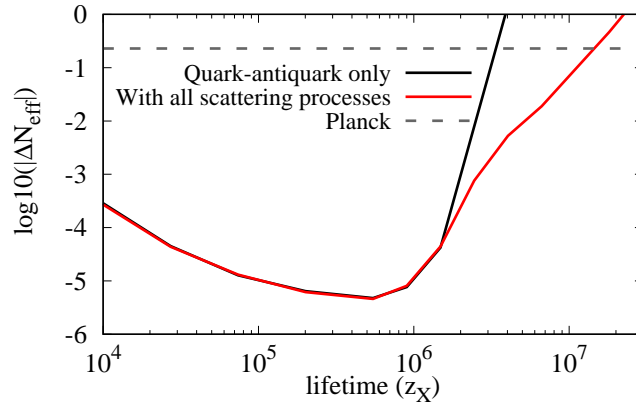


Figure 12: $2\text{-}\sigma$ Constraints on $|\Delta N_{\text{eff}}|$ from abundance of deuterium (overproduction of deuterium from destruction of helium) including only quark-antiquark pair production and including quark-antiquark as well as electron-positron pair production and neutrino-nucleon scattering. Energy of injected neutrino is 10^{12} GeV.

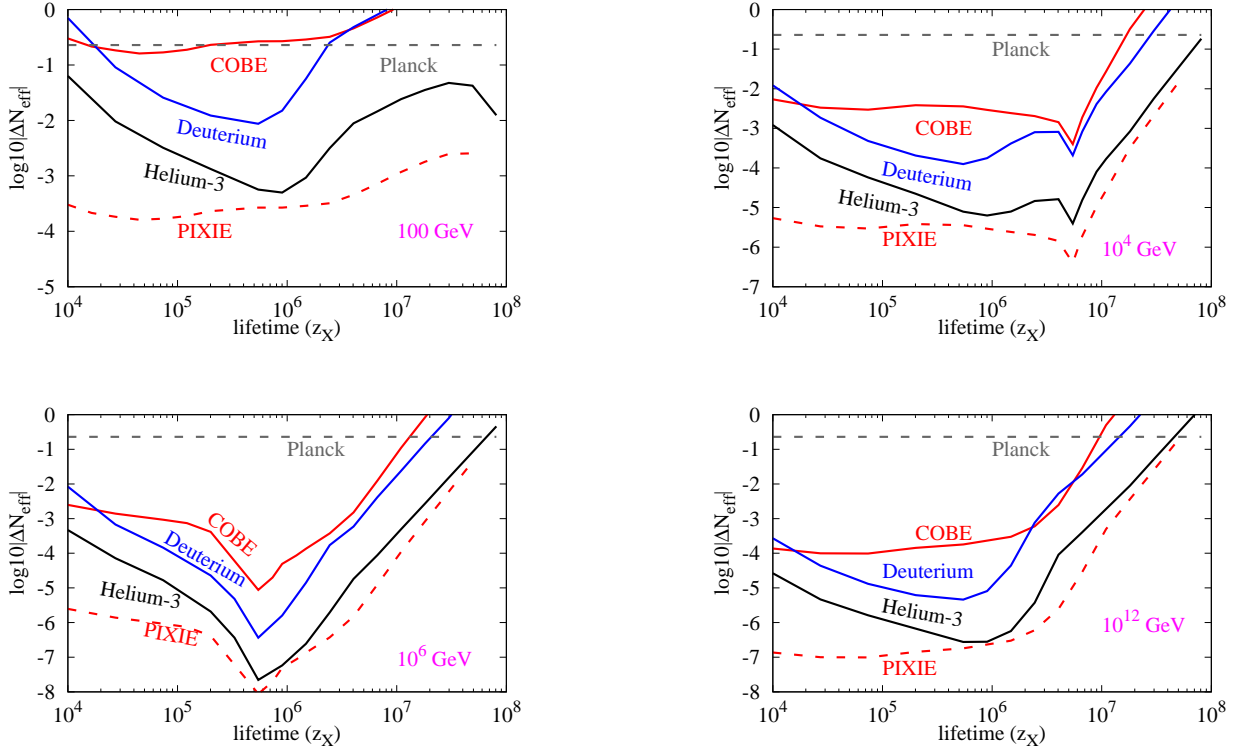


Figure 13: $2\text{-}\sigma$ Constraints on $|\Delta N_{\text{eff}}|$ from COBE and abundance of BBN elements for (a) 100 GeV (b) 10^4 GeV (c) 10^6 GeV (d) 10^{12} GeV neutrino energy. BBN constraints are from helium-4 destruction to helium-3 and deuterium. Also shown are projection for future experiment PIXIE [46].

standard model particles on background anti-neutrinos (neutrinos), electroweak showers from electroweak bremsstrahlung during decay or inelastic neutrino-nucleon scattering. The secondary electromagnetic energy injection can be constrained by CMB spectral distortions or light element abundance from BBN which indirectly puts constraints on the allowed fractional energy density of injected non-thermal neutrinos and the surviving extra neutrino energy density during recombination (ΔN_{eff}). We have shown that the CMB spectral distortion and the abundance of light elements strongly limit which sources or new physics can contribute to N_{eff} . In particular, we get constraints which are several orders of magnitude stronger compared to current *Planck* constraints on N_{eff} for models where the injected neutrinos have energy $\gtrsim 100$ GeV. We, therefore, rule out new physics which injects $\gtrsim 100$ GeV neutrinos in the early universe after neutrino decoupling as a significant source of deviation of N_{eff} from the standard ΛCDM value. To our knowledge, this is the first calculation which evolves N_{eff} from particle cascades in the early universe, does not assume N_{eff} to be a constant, and takes into account interaction of neutrinos with the background particles. We have also shown that

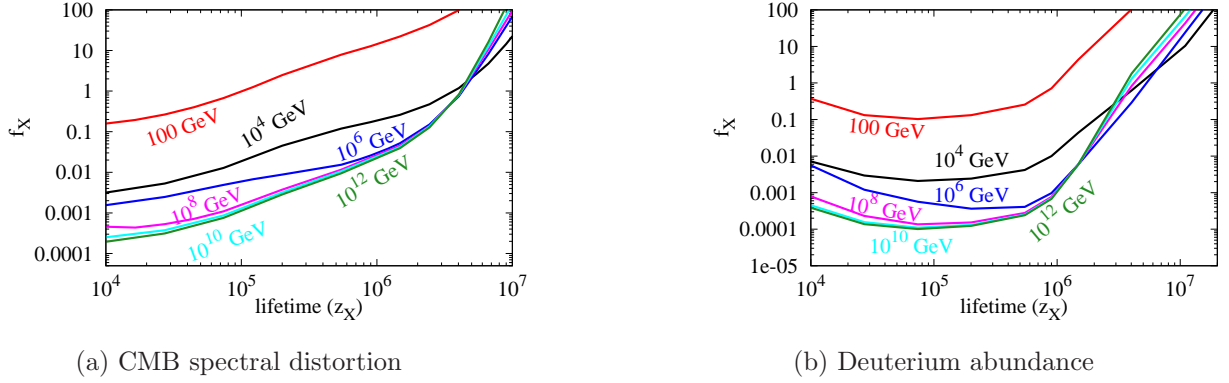


Figure 14: $2\text{-}\sigma$ constraints on fraction of decaying dark matter f_X , as a function of lifetime from (a) CMB spectral distortion (b) deuterium abundance (over-production of deuterium from destruction of helium-4). The labels correspond to the energy of initial neutrino injected.

with neutrino, we can probe deeper in redshift as compared to pure electromagnetic energy injection as the surviving neutrinos from $z \gtrsim 2 \times 10^6$ can deposit a fraction of their energy as electromagnetic energy at $z \lesssim 2 \times 10^6$. This opens up a new window to study energy injection history beyond CMB black body surface allowing us to peek into the CMB black body photosphere or the thermalization epoch.

7 Acknowledgements

We acknowledge the use of computational facilities of Department of Theoretical Physics at Tata Institute of Fundamental Research, Mumbai. This work was supported by Max Planck Partner Group for cosmology of Max Planck Institute for Astrophysics Garching at Tata Institute of Fundamental Research funded by Max-Planck-Gesellschaft. We acknowledge support of the Department of Atomic Energy, Government of India, under project no. 12-R&D-TFR-5.02-0200. SKA is grateful for financial support from the Royal Society and Prof. Jens Chluba for the invitation to University of Manchester, during which a part of this work was done.

A Computation of particles cascade

The evolution of particle spectra can be written as [63, 64],

$$\frac{\partial N_a^\alpha}{\partial t} = - \left(\sum_{\beta < \alpha} \sum_b P_{ab}^{\alpha\beta} N_a^\alpha \right) + \left(\sum_{\beta > \alpha} \sum_b P_{ba}^{\beta\alpha} N_b^\beta \right) + S_a^\alpha, \quad (\text{A.1})$$

where N_a^α, N_b^β are the number of particles of type a, b (where a and b can be neutrinos (anti-neutrinos), photons or electrons (positrons)) in the bin denoted by α, β with energy E_α and E_β

respectively, $P_{ab}^{\alpha\beta}$ is the rate of particle of type a to transfer from bin α to β and particle type b with $E_\beta < E_\alpha$ in a timestep, S_a^α is a source or sink function which can be non-zero for particle of type a injection or destruction in bin α at a particular timestep. For neutrinos above quark pair production threshold, $P_{ab}^{\alpha\beta}$ for $a=\text{neutrino}$ and $b=(\text{neutrino}, \text{photon}, \text{electron})$ can be obtained directly from **PYTHIA** data of [41]. The authors in [41] provide spectrum of secondary neutrinos, photons and electrons after hadronization of quark-antiquark pair from neutrino-antineutrino pair-production. For neutrino-nucleon scattering and electromagnetic processes, $P_{ab}^{\alpha\beta}$ can be computed from the cross-section of these processes. The expression for $P_{ab}^{\alpha\beta}$ is given by,

$$P_{ab}^{\alpha\beta} = \sum n_T c \frac{d\sigma_{ab}^{\alpha\beta}}{dE^\beta} \Delta E^\beta, \quad (\text{A.2})$$

where n_T is the number density of target particles for a particular scattering process, $\frac{d\sigma_{ab}^{\alpha\beta}}{dE^\beta}$ is the differential cross-section for a particle of type a in bin α to scatter to bin β as a particle of type b . The cross-section for neutrino-nucleon scattering and electromagnetic processes, used in this work, can be found in [17] and [29] respectively and references therein. For spectral distortion calculations, the energy of electromagnetic particles produced in a time step from quark hadronization and neutrino-nucleon scattering are just summed up and there is nothing else to be done for these particles. For BBN elements calculations, we ignore the time evolution of electromagnetic particles which just means putting left hand side of Eq. A.1 for these particles to be zero. This is the on-the-spot approximation which assumes that all the injected electromagnetic energy is deposited on time scales smaller than the Hubble time. By solving the resulting algebraic equations [29, 63, 64], we obtain the secondary electromagnetic spectrum and energy deposited as photo-dissociation of nuclei, from interaction of $\sim \text{GeV}$ energy electromagnetic particles with background photons, electrons and nuclei.

B Comparison of on-the-spot and full cascade calculations on constraints of abundance of light elements

We show the comparison of the simplified calculation with on-the-spot approximation with the full cascade calculation in Fig. 15. We plot the constraints obtained from helium-3 abundance for dark matter decay to monochromatic photon pairs with $z_X = 20000$. For photons with energy $\gtrsim \text{GeV}$, on-the-spot approximation is very good with only slightly stronger constraints compared to the full calculation.

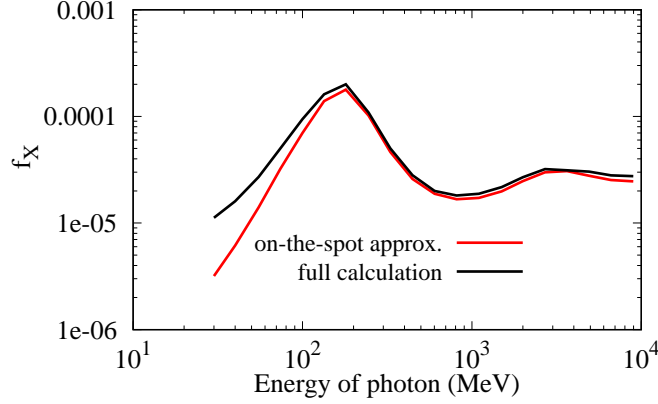


Figure 15: $2\text{-}\sigma$ constraint on f_X from helium-3 abundance for dark matter decay to monochromatic photon pairs as a function of photon’s energy. The lifetime of dark matter is $z_X = 20000$.

References

- [1] N. Aghanim et al. Planck 2018 results. VI. Cosmological parameters. *ArXiv e-prints*, July 2018. [arXiv:1807.06209](#), [ADS].
- [2] Scott Dodelson and Michael S. Turner. Nonequilibrium neutrino statistical mechanics in the expanding Universe. *Phys.Rev.D*, 46(8):3372–3387, October 1992. [DOI], [ADS].
- [3] Steen Hannestad and Jes Madsen. Neutrino decoupling in the early Universe. *Phys.Rev.D*, 52(4):1764–1769, August 1995. [arXiv:astro-ph/9506015](#), [DOI], [ADS].
- [4] A. D. Dolgov, S. H. Hansen, and D. V. Semikoz. Non-equilibrium corrections to the spectra of massless neutrinos in the early universe. *Nuclear Physics B*, 503:426–444, February 1997. [arXiv:hep-ph/9703315](#), [DOI], [ADS].
- [5] Nickolay Y. Gnedin and Oleg Y. Gnedin. Cosmological Neutrino Background Revisited. *ApJ*, 509(1):11–15, December 1998. [arXiv:astro-ph/9712199](#), [DOI], [ADS].
- [6] A. D. Dolgov, S. H. Hansen, and D. V. Semikoz. Non-equilibrium corrections to the spectra of massless neutrinos in the early universe. *Nuclear Physics B*, 543(1-2):269–274, March 1999. [arXiv:hep-ph/9805467](#), [DOI], [ADS].
- [7] A. D. Dolgov. Neutrinos in cosmology. *Physics Reports*, 370(4-5):333–535, November 2002. [arXiv:hep-ph/0202122](#), [DOI], [ADS].
- [8] G. Mangano, G. Miele, S. Pastor, and M. Peloso. A precision calculation of the effective number of cosmological neutrinos. *Physics Letters B*, 534(1-4):8–16, May 2002. [arXiv:astro-ph/0111408](#), [DOI], [ADS].
- [9] Gianpiero Mangano, Gennaro Miele, Sergio Pastor, Teguyco Pinto, Ofelia Pisanti, and Pasquale D. Serpico. Relic neutrino decoupling including flavour oscillations. *Nuclear Physics B*, 729(1-2):221–234, November 2005. [arXiv:hep-ph/0506164](#), [DOI], [ADS].

- [10] Jeremiah Birrell, Cheng Tao Yang, and Johann Rafelski. Relic neutrino freeze-out: Dependence on natural constants. *Nuclear Physics B*, 890:481–517, January 2015. [arXiv:1406.1759](#), [\[DOI\]](#), [\[ADS\]](#).
- [11] Pablo F. de Salas and Sergio Pastor. Relic neutrino decoupling with flavour oscillations revisited. *JCAP*, 2016(7):051, July 2016. [arXiv:1606.06986](#), [\[DOI\]](#), [\[ADS\]](#).
- [12] S. Gariazzo, P. F. de Salas, and S. Pastor. Thermalisation of sterile neutrinos in the early universe in the 3+1 scheme with full mixing matrix. *JCAP*, 2019(7):014, July 2019. [arXiv:1905.11290](#), [\[DOI\]](#), [\[ADS\]](#).
- [13] Kensuke Akita and Masahide Yamaguchi. A precision calculation of relic neutrino decoupling. *arXiv e-prints*, page arXiv:2005.07047, May 2020. [arXiv:2005.07047](#), [\[ADS\]](#).
- [14] V. Berezhinsky, M. Kachelrieß, and S. Ostapchenko. Electroweak Jet Cascading in the Decay of Superheavy Particles. *Phys.Rev.Lett*, 89(17):171802, October 2002. [arXiv:hep-ph/0205218](#), [\[DOI\]](#), [\[ADS\]](#).
- [15] M. Kachelrieß and P. D. Serpico. Model-independent dark matter annihilation bound from the diffuse gamma ray flux. *Phys.Rev.D*, 76(6):063516, September 2007. [arXiv:0707.0209](#), [\[DOI\]](#), [\[ADS\]](#).
- [16] Paolo Ciafaloni, Denis Comelli, Antonio Riotto, Filippo Sala, Alessandro Strumia, and Alfredo Urbano. Weak corrections are relevant for dark matter indirect detection. *JCAP*, 2011(3):019, March 2011. [arXiv:1009.0224](#), [\[DOI\]](#), [\[ADS\]](#).
- [17] Raj Gandhi, Chris Quigg, Mary Hall Reno, and Ina Sarcevic. Ultrahigh-energy neutrino interactions. *Astroparticle Physics*, 5(2):81–110, August 1996. [arXiv:hep-ph/9512364](#), [\[DOI\]](#), [\[ADS\]](#).
- [18] Amanda Cooper-Sarkar, Philipp Mertsch, and Subir Sarkar. The high energy neutrino cross-section in the Standard Model and its uncertainty. *Journal of High Energy Physics*, 2011:42, August 2011. [arXiv:1106.3723](#), [\[DOI\]](#), [\[ADS\]](#).
- [19] J. A. Formaggio and G. P. Zeller. From eV to EeV: Neutrino cross sections across energy scales. *Reviews of Modern Physics*, 84(3):1307–1341, July 2012. [arXiv:1305.7513](#), [\[DOI\]](#), [\[ADS\]](#).
- [20] Paolo Gondolo, Graciela Gelmini, and Subir Sarkar. Cosmic neutrinos from unstable relic particles. *Nuclear Physics B*, 392(1):111–133, March 1993. [arXiv:hep-ph/9209236](#), [\[DOI\]](#), [\[ADS\]](#).
- [21] Esteban Roulet. Ultrahigh energy neutrino absorption by neutrino dark matter. *Phys.Rev.D*, 47(12):5247–5252, June 1993. [\[DOI\]](#), [\[ADS\]](#).
- [22] Y. B. Zeldovich and R. A. Sunyaev. The Interaction of Matter and Radiation in a Hot-Model Universe. *ApSS*, 4:301–316, July 1969. [\[DOI\]](#), [\[ADS\]](#).
- [23] R. A. Sunyaev and Y. B. Zeldovich. The interaction of matter and radiation in the hot model of the Universe, II. *ApSS*, 7:20–30, April 1970. [\[DOI\]](#), [\[ADS\]](#).
- [24] A. F. Illarionov and R. A. Siuniaev. Comptonization, the background-radiation spectrum, and the thermal history of the universe. *Soviet Astronomy*, 18:691–699, June 1975. [\[ADS\]](#).
- [25] C. Burigana, L. Danese, and G. de Zotti. Formation and evolution of early distortions of the microwave background spectrum - A numerical study. *A&A*, 246:49–58, June 1991. [\[ADS\]](#).

- [26] J. Chluba and R. A. Sunyaev. The evolution of CMB spectral distortions in the early Universe. *MNRAS*, 419:1294–1314, January 2012. [arXiv:1109.6552](#), [DOI], [ADS].
- [27] R. Khatri and R. A. Sunyaev. Beyond y and μ : the shape of the CMB spectral distortions in the intermediate epoch, $1.5 \times 10^4 \lesssim z \lesssim 2 \times 10^5$. *JCAP*, 9:016, September 2012. [arXiv:1207.6654](#), [DOI], [ADS].
- [28] J. Chluba. Green’s function of the cosmological thermalization problem. *MNRAS*, 434:352–357, September 2013. [arXiv:1304.6120](#), [DOI], [ADS].
- [29] Sandeep Kumar Acharya and Rishi Khatri. Rich structure of nonthermal relativistic CMB spectral distortions from high energy particle cascades at redshifts $z \lesssim 2 \times 10^5$. *Phys.Rev.D*, 99(4):043520, Feb 2019. [arXiv:1808.02897](#), [DOI], [ADS].
- [30] Sandeep Kumar Acharya and Rishi Khatri. New CMB spectral distortion constraints on decaying dark matter with full evolution of electromagnetic cascades before recombination. *Phys.Rev.D*, 99(12):123510, June 2019. [arXiv:1903.04503](#), [DOI], [ADS].
- [31] R. Khatri and R. A. Sunyaev. Creation of the CMB spectrum: precise analytic solutions for the blackbody photosphere. *JCAP*, 6:38, 2012. [DOI], [ADS].
- [32] J. Chluba. Refined approximations for the distortion visibility function and μ -type spectral distortions. *MNRAS*, 440(3):2544–2563, May 2014. [arXiv:1312.6030](#), [DOI], [ADS].
- [33] J. Ellis, D. V. Nanopoulos, and S. Sarkar. The cosmology of decaying gravitinos. *Nuclear Physics B*, 259:175–188, September 1985. [DOI], [ADS].
- [34] J. Ellis, G. B. Gelmini, J. L. Lopez, D. V. Nanopoulos, and S. Sarkar. Astrophysical constraints on massive unstable neutral relic particles. *Nuclear Physics B*, 373:399–437, April 1992. [DOI], [ADS].
- [35] M. Kawasaki and T. Moroi. Electromagnetic Cascade in the Early Universe and Its Application to the Big Bang Nucleosynthesis. *ApJ*, 452:506, Oct 1995. [arXiv:astro-ph/9412055](#), [DOI], [ADS].
- [36] Vivian Poulin and Pasquale Dario Serpico. Nonuniversal BBN bounds on electromagnetically decaying particles. *Phys.Rev.D*, 91(10):103007, May 2015. [arXiv:1503.04852](#), [DOI], [ADS].
- [37] Masahiro Kawasaki, Kazunori Kohri, Takeo Moroi, and Yoshitaro Takaesu. Revisiting big-bang nucleosynthesis constraints on long-lived decaying particles. *Phys.Rev.D*, 97(2):023502, Jan 2018. [arXiv:1709.01211](#), [DOI], [ADS].
- [38] Marco Hufnagel, Kai Schmidt-Hoberg, and Sebastian Wild. BBN constraints on MeV-scale dark sectors. Part II: Electromagnetic decays. *Journal of Cosmology and Astro-Particle Physics*, 2018(11):032, Nov 2018. [arXiv:1808.09324](#), [DOI], [ADS].
- [39] Lindsay Forestell, David E. Morrissey, and Graham White. Limits from BBN on light electromagnetic decays. *Journal of High Energy Physics*, 2019(1):74, Jan 2019. [arXiv:1809.01179](#), [DOI], [ADS].
- [40] Sandeep Kumar Acharya and Rishi Khatri. CMB anisotropy and BBN constraints on pre-recombination decay of dark matter to visible particles. *JCAP*, 2019(12):046, Dec 2019. [arXiv:1910.06272](#), [DOI], [ADS].
- [41] Marco Cirelli, Gennaro Corcella, Andi Hektor, Gert Hütsi, Mario Kadastik, Paolo Panci, Martti

Raidal, Filippo Sala, and Alessandro Strumia. PPC 4 DM ID: a poor particle physicist cookbook for dark matter indirect detection. *JCAP*, 2011(3):051, March 2011. [arXiv:1012.4515](#), [DOI], [ADS].

- [42] D. J. Fixsen, E. S. Cheng, D. A. Cottingham, Jr. Eplee, R. E., T. Hewagama, R. B. Isaacman, K. A. Jensen, J. C. Mather, D. L. Massa, S. S. Meyer, P. D. Noerdlinger, S. M. Read, L. P. Rosen, R. A. Shafer, A. R. Trenholme, R. Weiss, C. L. Bennett, N. W. Boggess, D. T. Wilkinson, and E. L. Wright. Calibration of the COBE FIRAS Instrument. *ApJ*, 420:457, January 1994. [DOI], [ADS].
- [43] J. C. Mather, E. S. Cheng, D. A. Cottingham, R. E. Eplee, Jr., D. J. Fixsen, T. Hewagama, R. B. Isaacman, K. A. Jensen, S. S. Meyer, P. D. Noerdlinger, S. M. Read, L. P. Rosen, R. A. Shafer, E. L. Wright, C. L. Bennett, N. W. Boggess, M. G. Hauser, T. Kelsall, S. H. Moseley, Jr., R. F. Silverberg, G. F. Smoot, R. Weiss, and D. T. Wilkinson. Measurement of the cosmic microwave background spectrum by the COBE FIRAS instrument. *ApJ*, 420:439–444, January 1994. [DOI], [ADS].
- [44] D. J. Fixsen, E. S. Cheng, J. M. Gales, J. C. Mather, R. A. Shafer, and E. L. Wright. The Cosmic Microwave Background Spectrum from the Full COBE FIRAS Data Set. *ApJ*, 473:576, December 1996. [arXiv:astro-ph/9605054](#), [DOI], [ADS].
- [45] D. J. Fixsen and J. C. Mather. The Spectral Results of the Far-Infrared Absolute Spectrophotometer Instrument on COBE. *ApJ*, 581:817–822, December 2002. [DOI], [ADS].
- [46] A. Kogut, D. J. Fixsen, D. T. Chuss, J. Dotson, E. Dwek, M. Halpern, G. F. Hinshaw, S. M. Meyer, S. H. Moseley, M. D. Seiffert, D. N. Spergel, and E. J. Wollack. The Primordial Inflation Explorer (PIXIE): a nulling polarimeter for cosmic microwave background observations. *JCAP*, 7:025, July 2011. [arXiv:1105.2044](#), [DOI], [ADS].
- [47] John Gratsias, Robert J. Scherrer, and David N. Spergel. Indirect photofission of light elements from high-energy neutrinos in the early universe. *Physics Letters B*, 262(2-3):298–302, June 1991. [DOI], [ADS].
- [48] Andrew A. de Laix and Robert J. Scherrer. Improved cosmological constraints on neutrino-producing decaying particles. *Phys.Rev.D*, 48(2):562–566, July 1993. [DOI], [ADS].
- [49] Kenneth M. Nollett and Gary Steigman. BBN and the CMB constrain light, electromagnetically coupled WIMPs. *Phys.Rev.D*, 89(8):083508, April 2014. [arXiv:1312.5725](#), [DOI], [ADS].
- [50] IceCube collaboration. First Observation of PeV-Energy Neutrinos with IceCube. *Phys.Rev.Lett*, 111(2):021103, July 2013. [arXiv:1304.5356](#), [DOI], [ADS].
- [51] Laura Covi, Michael Grefe, Alejandro Ibarra, and David Tran. Neutrino signals from dark matter decay. *JCAP*, 2010(4):017, April 2010. [arXiv:0912.3521](#), [DOI], [ADS].
- [52] Brian Feldstein, Alexander Kusenko, Shigeki Matsumoto, and Tsutomu T. Yanagida. Neutrinos at IceCube from heavy decaying dark matter. *Phys.Rev.D*, 88(1):015004, July 2013. [arXiv:1303.7320](#), [DOI], [ADS].
- [53] Luis A. Anchordoqui, Vernon Barger, Haim Goldberg, Xing Huang, Danny Marfatia, Luiz H. M. da Silva, and Thomas J. Weiler. IceCube neutrinos, decaying dark matter, and the Hubble constant. *Phys.Rev.D*, 92(6):061301, September 2015. [arXiv:1506.08788](#), [DOI], [ADS].
- [54] Nagisa Hiroshima, Ryuichiro Kitano, Kazunori Kohri, and Kohta Murase. High-energy

- neutrinos from multibody decaying dark matter. *Phys.Rev.D*, 97(2):023006, January 2018. [arXiv:1705.04419](#), [DOI], [ADS].
- [55] Torbjörn Sjöstrand, Stephen Mrenna, and Peter Skands. PYTHIA 6.4 physics and manual. *Journal of High Energy Physics*, 2006(5):026, May 2006. [arXiv:hep-ph/0603175](#), [DOI], [ADS].
- [56] Torbjörn Sjöstrand, Stefan Ask, Jesper R. Christiansen, Richard Corke, Nishita Desai, Philip Ilten, Stephen Mrenna, Stefan Prestel, Christine O. Rasmussen, and Peter Z. Skands. An introduction to PYTHIA 8.2. *Computer Physics Communications*, 191:159–177, Jun 2015. [arXiv:1410.3012](#), [DOI], [ADS].
- [57] Jens Chluba, Andrea Ravenni, and Sandeep Kumar Acharya. Thermalization of large energy release in the early Universe. *arXiv e-prints*, page arXiv:2005.11325, May 2020. [arXiv:2005.11325](#), [ADS].
- [58] Vimal Simha and Gary Steigman. Constraining the early-Universe baryon density and expansion rate. *JCAP*, 2008(6):016, June 2008. [arXiv:0803.3465](#), [DOI], [ADS].
- [59] Richard H. Cyburt, Brian D. Fields, Keith A. Olive, and Tsung-Han Yeh. Big bang nucleosynthesis: Present status. *Reviews of Modern Physics*, 88(1):015004, Jan 2016. [arXiv:1505.01076](#), [DOI], [ADS].
- [60] Erik Aver, Keith A. Olive, and Evan D. Skillman. The effects of He I λ 10830 on helium abundance determinations. *Journal of Cosmology and Astro-Particle Physics*, 2015(7):011, Jul 2015. [arXiv:1503.08146](#), [DOI], [ADS].
- [61] T. M. Bania, Robert T. Rood, and Dana S. Balser. The cosmological density of baryons from observations of 3He+ in the Milky Way. *Nature*, 415, 2002. [DOI].
- [62] Erich Holtmann, M. Kawasaki, K. Kohri, and Takeo Moroi. Radiative decay of a long-lived particle and big-bang nucleosynthesis. *Phys.Rev.D*, 60(2):023506, July 1999. [arXiv:hep-ph/9805405](#), [DOI], [ADS].
- [63] Toru Kanzaki and Masahiro Kawasaki. Electron and photon energy deposition in the Universe. *Phys.Rev.D*, 78(10):103004, Nov 2008. [arXiv:0805.3969](#), [DOI], [ADS].
- [64] T. R. Slatyer, N. Padmanabhan, and D. P. Finkbeiner. CMB constraints on WIMP annihilation: Energy absorption during the recombination epoch. *Phys.Rev.D*, 80(4):043526, August 2009. [arXiv:0906.1197](#), [DOI], [ADS].